Bioactive biodegradable polycitrate nanoclusters enhances the myoblast differentiation and *in vivo* skeletal muscle regeneration *via* p38 MAPK signaling pathway

Yi Guo[a,e,1], Min Wang[a,1], Juan Ge[a], Wen Niu[a], Mi Chen[a], Wei Cheng[a], Bo Lei[a,b,c,d,*]

[a] *Frontier Institute of Science and Technology, Xi'an Jiaotong University, Xi'an, 710054, China*
[b] *Key Laboratory of Shaanxi Province for Craniofacial Precision Medicine Research, College of Stomatology, Xi'an Jiaotong University, Xi'an, 710054, China*
[c] *National and Local Joint Engineering Research Center of Biodiagnosis and Biotherapy, The Second Affiliated Hospital of Xi'an Jiaotong University, Xi'an, 710000, China*
[d] *Instrument Analysis Center, Xi'an Jiaotong University, Xi'an, 710054, China*
[e] *Department of Biomedical Engineering, University of Michigan, Ann Arbor, MI, 48109, United States*

ARTICLE INFO

ABSTRACT

Complete skeletal muscle repair and regeneration due to severe large injury or disease is still a challenge. Biochemical cues are critical to control myoblast cell function and can be utilized to develop smart biomaterials for skeletal muscle engineering. Citric acid-based biodegradable polymers have received much attention on tissue engineering, however, their regulation on myoblast cell differentiation and mechanism was few investigated. Here, we find that citrate-based polycitrate-polyethylene glycol-polyethylenimine (POCG-PEI600) nanoclusters can significantly enhance the *in vitro* myoblast proliferation by probably reinforcing the mitochondrial number, promote the myotube formation and full-thickness skeletal muscle regeneration *in vivo* by activating the myogenic biomarker genes expression of *Myod* and *Mhc*. POCG-PEI600 nanoclusters could also promote the phosphorylation of p38 in MAP kinases (MAPK) signaling pathway, which led to the promotion of the myoblast differentiation. The *in vivo* skeletal muscle loss rat model also confirmed that POCG-PEI600 nanoclusters could significantly improve the angiogenesis, myofibers formation and complete skeletal muscle regeneration. POCG-PEI600 nanocluster could be also biodegraded into small molecules and eliminated *in vivo*, suggesting their high biocompatibility and biosafety. This study could provide a bioactive biomaterial-based strategy to repair and regenerate skeletal muscle tissue.

1. Introduction

Skeletal muscle tissues are often injured by toxic chemicals, biological factors, physical destructions and other skeletal muscle diseases [1–4]. For skeletal muscle tissue repair, nowadays, autografts, allografts and artificial grafts are commonly therapies methods in clinic [5,6]. However, clinical treatment strategies also possess the disadvantages, such as the shortcoming transplanting host muscle tissue, the high cost, site morbidity, long operative time, immune rejection and poor rehabilitation [7,8]. Therefore, effective skeletal muscle tissue repair strategies are in high requirement to improve the life quality and therapeutic process.

As compared to biological techniques, bioactive and biocompatible biomaterials-based strategies without therapeutics have shown very promising application in various tissue regeneration and cancer therapy [9–13]. As the skeletal tissue regeneration, the rapid proliferation and myogenic differentiation and myotube formation of muscle satellite cells plays the most important role [14,15]. Up to now, conductive biomaterials such as graphene, carbon nanotube and semiconductor polymers have exhibited that they can enhance the myogenic differentiation of myoblasts [16–20]. Our previous studies also demonstrated that the conductive nanocomposites and gold/silver nanoparticles could effectively regulate the myotube formation and promote the *in vivo* skeletal muscle tissue regeneration [21]. However, most of the reported biomaterials are not biodegradable, which was not desirable *in vivo* skeletal muscle regeneration. It was very necessary to develop novel bioactive materials with controlled biodegradation and biocompatibility for efficient skeletal muscle tissue regeneration.

Citric acid-based polymers such as polycitrate biomedical elastomers (PC) have attracted much attention in regeneration medicine, because of their biomimetic mechanical behavior and biodegradation and biocompatibility [22–27]. The PC-based elastomers possess the similar viscoelastomeric behavior with native soft tissues, and showed promising results in vascular tissue engineering [28,29]. Through molecular hybridization method, our group also developed a series of multifunctional PC-based biomaterials for potential gene delivery, tissue regeneration and bioimaging [30,31]. Recently, PC-based biomaterials also showed special advantages on enhancing the osteogenic differentiation of stem cells and promoting the skeletal muscle tissue regeneration [32–34]. Recently, our group further found that polycitrate-polyethylene glycol-polyethylenimine copolymer could significantly enhance the cell viability and proliferation of myoblast (C2C12) [31]. The myogenic differentiation and the myotube formation of myoblast were significantly depended on the cell proliferation [35]. Therefore, it is very interesting to investigate if POCG-PEI600 copolymer could induce the myogenic differentiation of C2C12, enhancing the myotube formation and skeletal muscle regeneration *in vivo*. Additionally, how the POCG-PEI600 copolymer and cells interact with each other at the molecular level are still not clear. Several signaling pathways, such as Wnt, Notch, NF-kB, ERK1/2, FGF and TGF-β are responsible for regulating general skeletal muscle formation and reconstruction [36–39]. What's more, the *p38* MAPK family is the signal transducers that also promote muscle differentiation *in vitro* and influence the skeletal muscle growth and repair *in vivo*, but only p38 MAPK γ directly affects the myogenic transcription factors of the Myod family [40,41]. Therefore, it was speculated that the POCG-PEI600 could regulate the C2C12 myoblast differentiation *via* influencing p38 MAPK γ signaling pathway. This hypothesis was demonstrated through analyzing the expressions of proteins and genes related with p38a MAPK signaling pathway, after interaction with POCG-PEI600 nanocopolymer and inhibitor (SB 203580).

In this study, we synthesized citric acid-based polycitrate-polyethylene glycol-polyethylenimine (POCG-PEI600) nanocopolymer and investigated their effect on the myogenic differentiation and related molecular mechanism and *in vivo* skeletal muscle tissue regeneration. The detailed effects of POCG-PEI600 on the proliferation, myotube formation, myogenic proteins and genes expression *in vitro* of myoblasts (C2C12), *in vivo* skeletal muscle tissue regeneration was also studied.

2. Materials and methods

2.1. Materials

2-(N-Morpholino) ethanesulfonic Acid (MES, 99%) N-Hydroxysuccinimide (NHS, 98%) and 1-(3-Dimethylaminopropyl)-3-ethylcarbodiimide hydrochloride (EDC, 99%) were obtained from J&K Scientific. Ascorbic acid, β-glycerophosphate, paraformaldehyde, Triton X-100, dexamethasone, citric acid (99%), sodium hydroxide (NaOH),1, 8-Octanediol (98%), hydrochloric acid (37%), polyethylene glycol (PEG) (1 kDa) and branched polyethylenimine (PEI) (600Da) were purchased from Sigma-Aldrich. 4′-6-diamidino-2-phenylindole (DAPI), LIVE/DEAD staining kit, BCA protein assay kit, SDS-PAGE gels, reverse transcription reagent kit, Trizol, secondary antibodies and Alamar Blue® kit were bought from Invitrogen. Horse serum and phosphate buffered saline (PBS), Dulbecco's Modified Eagle Medium (DMEM) and antibiotic-antimycotic solution were purchased from GIBCO. Fetal bovine serum was bought from Bioind. Propidiumiodide (PI) and mito-tracker were obtained from Thermo Fisher Scientific. Phosphor-p38 and p38 antibodies were purchased from cell signaling. MYOD, myosin heavy chain (MHC) and GAPDH antibodies were obtained from Abcam.

2.2. Synthesis of POCG-PEI600

The POCG-PEI600 was synthesized through the reaction of POCG and PEI-600. The POCG polymer was synthesized using citric acid (CA), 1, 8-octanediol (OD) and polyethylene glycol (PEG) by melt-derived polymerization. Then POCG was dissolved by EDC in MES buffer anhydrous for 30 min, and then added the PEI600 under stirring for 24 h at room temperature. The mixture was purified by dialysis for 2 days. The final POCG-PEI600 was obtained after freeze-drying. The detailed synthesis and procedures were available in previous paper [31,42].

2.3. Myoblasts cell culture, proliferation and cellular uptake evaluations

C2C12 is a model cell line that has been widely used to study the skeletal muscle regeneration. C2C12 mouse myoblast cell lines were purchased from the American Type Culture Collection (Rockville, MD) and routinely maintained in Dulbecco's Modified Eagle Medium (DMEM, GIBCO) supplemented with 10% fetal bovine serum (FBS, Bioind) and 1% antibiotic-antimycotic solution (including 10,000 U/mL penicillin, 10 mg/mL streptomycin, GIBCO) at 37 °C in a humidified atmosphere containing 5% CO_2. The medium was changed every 2–3 days. The initial proliferation was measured by using an Alamar blue® assay according to the manufacturer's instruction. The tissue culture polystyrene plates (TCP) were taken as blank control. Live/dead fluorescence staining kit was performed to observe the C2C12 cell viability. Red color represented dead cells and green color showed the live cells. The cellular uptake studies of POCG-PEI600 and beta-cyclodextrin *in vitro* were determined by a confocal laser scanning microscope (CLSM, FV1200, Olympus). The nucleus was stained as red using PI and the POCG-PEI600 showed the inherent blue fluorescence. POCG and PEI600 was used the control respectively. The experimental details were presented in supporting information.

2.4. Mito-tracker green fluorescent staining

C2C12 skeletal myoblasts were cultured on 14 mm round glass cover slips as above. Firstly, the cells were seeded on the cover slips and cultured in growth medium for 12 h. Next, in order to investigate the effect of POCG-PEI600 for mitochondria, the p38 MAPK signaling pathway inhibitor SB203580 (5 μM) was added into medium [43]. Then the cells were incubated with POCG-PEI600, POCG and PEI600 (40 μg/mL) for 7 days. Subsequently, the medium was removed and rinsed with PBS; incubating the mito-tracker (1:10,000; Thermo Fisher Scientific) for 60 min. Finally, the cells were observed by a laser confocal fluorescent microscope (CLSM, Olympus FV1200).

2.5. Myogenic differentiation analysis

C2C12 skeletal myoblasts were seeded at a density of 8000 cells/cm^2 on 24-well plates for12 h. To study the myogenic differentiation mechanism of C2C12 skeletal myoblasts induced by POCG-PEI600, we added the SB203580 (5 μM) to the differentiation medium (DMEM + 2% horse serum). Then the cells were continued to be cultured with the 40 μg/mL concentration of POCG-PEI600 for 7 days. The differentiation medium was renewed every two days. Two myogenic genes including *Myod* and myosin heavy chain (*Mhc*) was analyzed through the quantitative reverse transcription polymerase chain reaction (qRT-PCR) (Applied Biosystems 7500). *Gapdh* was used as the control and the relative quantification was calculated by the ΔΔCt method. The myotube formation of C2C12 cells under the effect of POCG-PEI600 was determined by the immunofluorescence staining. ImageJ software (National Institutes of Health, Bethesda, MD) was employed to obtain the myotube number, myotube length, myotube diameter and maturation index. The experimental details were presented in supporting information.
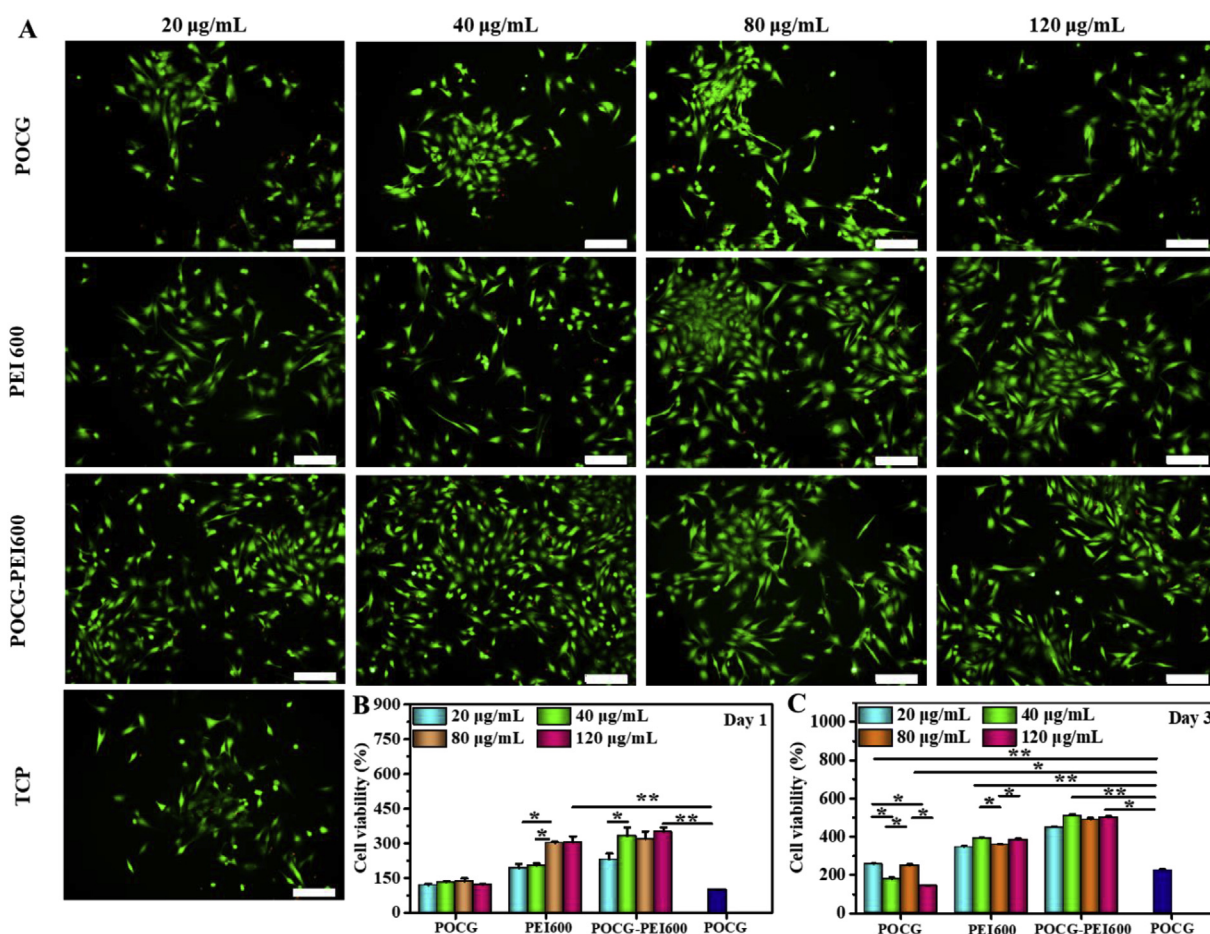
Fig. 1. C2C12 myoblasts viability evaluation after cultured with different copolymers for 1 to 3 days. (A) Live cell staining analysis (green fluorescence) on day 1 (scale bar: 200 μm); (B) C2C12 myoblasts viability on day 1, TCP was the blank control; (C) C2C12 myoblasts viability on day 3; All experiments were performed in triplicate (n = 4 per group, $*p < 0.05$; $**p < 0.01$), TCP was the blank control. POCG-PEI600 copolymers significantly enhanced the proliferation of C2C12 myoblasts. (For interpretation of the references to color in this figure legend, the reader is referred to the Web version of this article.)

2.6. Western blot evaluation

C2C12 were cultured in 60 mm plates with POCG-PEI600 for 7 days in myoblastic differentiation medium. After that, cell mass was wash three times with PBS, lysed for 30 min in ice-cold RIPA lysis buffer (20 mM Tris·HCl, pH = 8.0, 150 mM NaCl and 1% TritonX-100) and protease inhibitor cocktail and phosphatese inhibitor cocktail. Protein concentration was investigated using the BCA protein assay kit (Thermo Scientific). Equivalent protein was heated at 100 °C for 5 min in $5 \times$ loading buffer (Invitrogen). Proteins were separated by 8–12% SDS-PAGE gels (Invitrogen) and transferred to a polyvinylidene difluoride membrane by using a wet transfer apparatus. Membranes were blocked with 5% skim milk in TBS-T (20 mM Tris-HCl, pH = 7.5, 150 mM NaCl and 0.1% Tween) for 1 h at room temperature and incubated with the following primary antibodies overnight: p38 (1:1000; Cell signaling), phosphor-p38 (1:1000; Cell signaling), MYOD (1:1000; Abcam, Cambridge, UK), MHC (1:1000; Abcam, Cambridge, UK), and GAPDH (1:1000; Abcam, Cambridge, UK). After being washed with TBS-T, membranes were incubated with secondary antibodies for 1 h. The secondary antibodies purchased from Invitrogen (Anti-mouse lgG and Anti-rabbit lgG). Proteins were visualized using the ECL detection kit (CWBIO, Beijing, China).

2.7. Skeletal muscle regeneration in vivo

The rat tibialis anterior muscle model was created on the female SD mice. The weight of female SD mice was 180 g–200 g. Each group was repeated with five female SD mice. The female SD mice were maintained under standard animal housing conditions. SD mice were divided into three groups randomly. Animals were anaesthetized with 2% inhalation of isoflurane. The tibialis anterior muscle was exposed by cutting anterolateral skin. A 5 mm × 3 mm x 2 mm (length, width and depth) rectangular-shaped defect was created on the skeletal muscle. The thermal-responsive hybrid hydrogel was fabricated (F127-POCG-PEI600), in which the final concentration of POCG-PEI600 in hydrogels was 40 μg/mL and the concentration of F127 was 25 wt%. The hydrogels were injected in the muscle defects. The Empty group and pure F127 hydrogel group was considered as the controls respectively. After 7 days and 28 days, for examination of new muscle formation, the defect skeletal muscle were fixed with formalin, infiltrate by resin, and the tissue slices were observed under light microscope after Hematoxylin-Eosin-staining (H.E. staining).

2.8. Statistical analyses

All variables were tested in three independent cultures for each experiment. All data were expressed as mean ± standard deviation. Statistical comparisons were carried out using a one-way analysis of variance (ANOVA; SAS Institute Inc., Cary, NC, USA), followed by a Bonferroni test for multiple comparisons. A value of $*p < 0.05$, $**p < 0.01$ were considered to be statistically significant.

3. Results and discussion

3.1. Myoblast biocompatibility evaluation of POCG-PEI600

To decrease the possible cytotoxicity of PEI polymer, PEI with an average molecular weight of 600 was used to synthesize POCG-PEI600. The successful synthesis and chemical structures of POCG-PEI600 were determined by previous study, ^{1}H NMR and FT-IR analysis in Fig. S1 [31]. The presence of peaks between 3.9 and 4.3 ppm (–CH$_2$–) indicated the successful synthesis of POCG. The presence of double peaks at 3.0 and 3.1 ppm (–CONHCH$_2$–) belonged to the methylene protons of PEI600, suggesting the formation of POCG-PEI600 [31]. The FT-IR was also used to confirm the chemical structure of prepared polymers. The double peaks at 2800-3000 cm^{-1} represented the methylene (–CH$_2$–). The eater bonds (–COO–) in POCG and amido bond (–CONH–) in POCG-PEI600 were showed at 1600-1800 cm^{-1}. The characteristic peaks at 1500-1600 cm^{-1} were assigned to amide (–NH–) of PEI600 (Fig. S1). The transmitted electron microscope (TEM) images showed that POCG-PEI600 form a monodispersed spherical nanoscale size of 200 nm in a cell culture medium containing 10% FBS (Fig. S2) The hydrodynamic diameter of POCG-PEI600 was about 197 nm with a Zeta potential of 21.6 mV (Table S1). The result of particle size was similar by TEM and hydrodynamic diameter methods.

Firstly, whether POCG-PEI600 could promote cell viability and proliferation was studied. After cultured with POCG-PEI600 at different concentrations (0, 20, 40, 80, 120 μg/mL), C2C12 cells showed different cell viability and proliferation (Fig. 1). After cultivation for 1 day and 3 days, most of the cells were alive (green), while few were dead (red), and all cells exhibited a normal morphology, which indicated that POCG-PEI600 had a good biocompatibility *in vitro* (Fig. 1A). Furthermore, the cell proliferation behavior was quantitatively analyzed by Alamar blue assay. On day 1, relatively to the TCP control, cells showed a significantly high proliferation in PEI600/POCG-PEI600 group (Fig. 1B). The cell proliferation of POCG group was better than TCP group. Under the same concentration (40 μg/mL), the cell viability in POCG-PEI600 group was significantly higher than other groups on day 1. On day 3, the cell viability in PEI600 and POCG-PEI600 groups maintained the same trend as day 1 at various concentrations (Fig. 1C). In contrast to day 1, the cellular activity of POCG group (20 and 80 μg/mL) was significantly increased compared with TCP group. The cell viability was also related to the concentration of POCG-PEI600 and the high concentration contributed to the cell proliferation. However, no significant difference was found at concentration of 40–120 μg/mL. All these results demonstrated that POCG-PEI600 significantly enhanced the C2C12 myoblast proliferation which probably affected the myogenic differentiation. Based on the inherent fluorescence of POCG-PEI600 polymer, the cellular uptake in C2C12 cells was determined. The CLSM images with high magnification showed that POCG-PEI600 was distributed in cytoplasm (Fig. S3A, Fig. S3C). And the beta-cyclodextrin as the inhibitor of caveolin was performed to show the cell uptake pathway of POCG-PEI600 in C2C12 cells. It was obvious found that no POCG-PEI600 was observed when the inhibitor was used (Fig. S3B, Fig. S3D), suggesting that the cellular uptake of C2C12 cells was probably *via* caveolin-mediated endocytosis pathway. In addition, previous reports also showed that p38 MAPK have a positive effect by the activation of PGC-1α for mitochondrial biogenesis [44]. And the activation of p38 MAPK can promote the behavior and function of mitochondria [45]. Therefore, the SB 203580 as the inhibitor of p38 MAPK signaling pathway and green mito-tracker staining were used to explain the effect of POCG-PEI600 on the mitochondria of C2C12 cells. It was clearly observed that strong positive green fluorescence staining was found in POCG-PEI600 group, as compared to TCP, POCG and PEI600 group (Fig. 2A). POCG-PEI600 treated C2C12 cells showed the significantly high mitochondrial number per cell compared with other groups (Fig. 2B). There was no significant difference in mitochondrial number per cell among the TCP, POCG and PEI groups. Under the effect

of SB 203580, it was observed that the inhibitor groups did not generate mature myotubes and the green fluorescence of the inhibitor groups was also a little less than normal group (Fig. S4A). However, the mitochondrial number per cell in POCG-PEI600 + SB203580 group was stronger comparing with TCP + SB203580, POCG + SB203580 and PEI600 +SB203580 (Fig. S4B). At the meanwhile, we found that the largest cell number of cells was POCG-PEI600 + SB203580 group compared with other inhibitor groups. This result suggested that the enhanced proliferation of C2C12 was probably because POCG-PEI600 could enhance the mitochondrial number.

3.2. Myogenic differentiation effect of POCG-PEI600

Skeletal muscle satellite cells grew and differentiated well, and finally the single nucleus round cells changed into the multinuclear cast myotube shape cells gradually. MHC protein immunofluorescence staining assay was used to visualize the morphology of the formed myotubes in C2C12 cells. Fig. 3 shows the results of immunofluorescence staining assay after incubation for 7 days. The myotube number, diameter, length and maturation index, were quantified by morphological analysis. The myotube maturation was quantified by determining the ratio of myotube number with more than 5 nuclei to the total myotube number (myotube maturation index). Compared with TCP control, PEI600 at the concentration of 40 μg/mL inhibited the MHC expression and POCG did not affect the MHC expression, and significantly high positive MHC staining was found in POCG-PEI600 group (Fig. 3A). As compared to TCP, POCG and PEI600, POCG-PEI600 demonstrated the significantly high myotube number, myotube length, myotube diameter and myotube maturation index (Fig. 3B–E). Additionally, the maturation index of POCG-PEI600 was as high as 80%.

We further investigated the influence of the POCG-PEI600 (40 μg/mL) on myogenic genes expression of C2C12 cells *in vitro*. *Myod* and *Mhc*, the early and late markers of myogenesis, were used to determine the myogenic differentiation at mRNA level. After culture for 7 days in normal medium, POCG-PEI600 showed the more than twice of TCP/POCG/PEI600 in the *Myod* gene expressions (Fig. 3F). The *Myod* gene expression of POCG and PEI600 was almost the same as TCP (Fig. 3F). In the meanwhile, *Myod* gene expression of POCG-PEI600 equaled triple that of TCP with differentiation medium (Fig. 3G). Subsequently, in normal medium, *Mhc* gene expression of POCG-PEI600 completely outclassed TCP, and almost 1.5 times than POCG/PEI600 group (Fig. 3F). The *Mhc* gene expression of POCG and PEI600 were more than three times as TCP (Fig. 3F). However, the *Mhc* expression of POCG-PEI600 was significantly twice of TCP with differentiation medium (Fig. 3G). Together, the results of real-time PCR clearly illustrated that POCG-PEI600 could significantly improve C2C12 myogenic differentiation through improving the *Myod* and *Mhc* expression. The enhanced myogenic differentiation performance for POCG-PEI600 was probably related with their high C2C12 viability since C2C12 cells have a higher tendency to differentiate at high confluence than at low confluence [46].

3.3. Myogenic differentiation mechanism analysis

The results described above showed that POCG-PEI600 could significantly enhance C2C12 cells proliferation and myogenic differentiation, however, the molecular mechanism was not clear. Here, based on our previous studies related with the nanomaterials guiding tissue regeneration, it was speculated that POCG-PEI600 may participate in the p38 MAPK γ signaling pathway which could affect myocyte fusion. To verify the possibility that whether p38 signaling activity is needed for muscle cell fusion induced by POCG-PEI600, C2C12 cells were incubated in DMEM with SB203580 (inhibitor) and 2% horse serum for 7 days. The relationship and process of p38 MAPK γ signaling pathway and POCG-PEI600 were shown in Scheme 1.

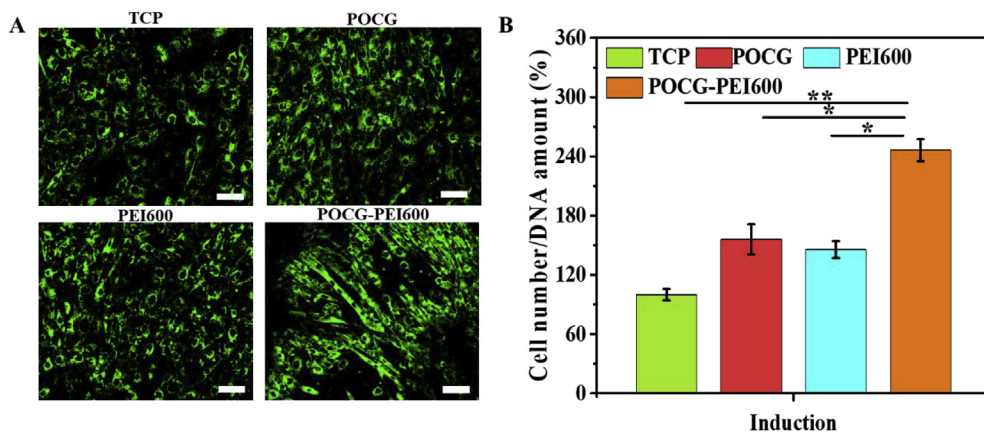In the continued presence of SB203580, few multinucleated

Fig. 2. Mitochondria staining in C2C12 cells after 7 days culture with various copolymers in myogenic differentiation medium. (A) Fluorescent staining of mitochondria by Mito-tracker (scale bar 200 μm); (B) Quantitative analysis of the mitochondrial amount per cell on Mito-tracker green fluorescent staining by image J. TCP was the blank control, all experiments were performed in triplicate (n = 4 per group, *$p < 0.05$, **$p < 0.01$). POCG-PEI600 copolymers significantly enhanced the mitochondrial number in C2C12 myoblasts. (For interpretation of the references to color in this figure legend, the reader is referred to the Web version of this article.)
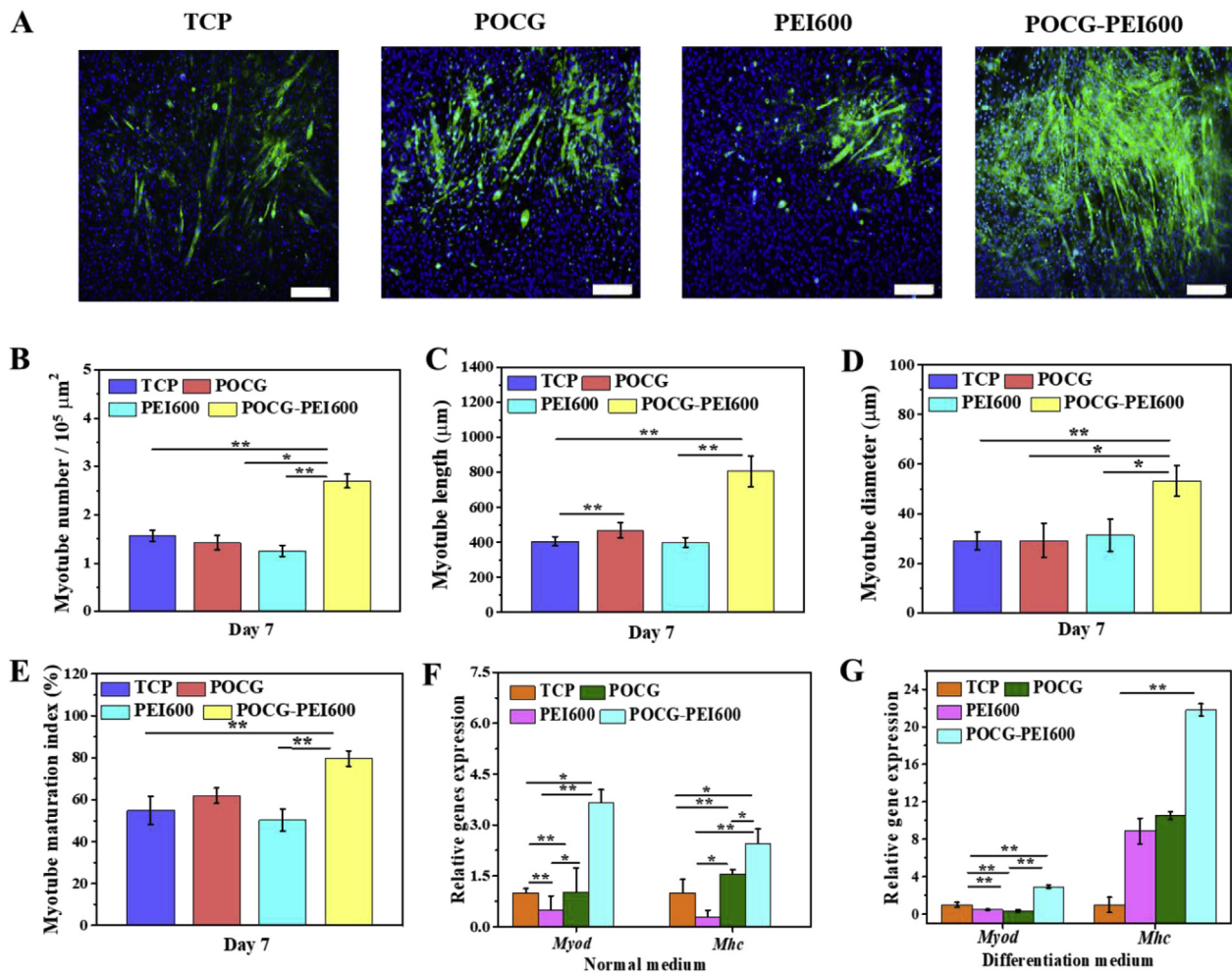

Fig. 3. *In vitro* myogenic differentiation evaluation of C2C12 myoblasts regulated by various copolymers (40 μg/mL). (A) Immunofluorescence staining of MHC protein (green) in C2C12 cells on day 7 in myogenic differentiation medium (scale bar 200 μm, cell nuclei: blue); (B–E) Quantitative analysis of myotube number per 10^5 mm^2 (B), myotube length (C), myotube diameter (D), and myotube maturation index (% myotubes with ≥5 nuclei) (E); (F–G) *Myod* and *Mhc* myogenic gene expression in normal medium (F) and myogenic differentiation medium (G). All experiments were performed in triplicate (n = 4 per group, *$p < 0.05$, **$p < 0.01$). POCG-PEI600 copolymers significantly enhanced the *in vitro* myotube formation and myogenic differentiation of C2C12 myoblasts. (For interpretation of the references to color in this figure legend, the reader is referred to the Web version of this article.)

myotubes were detected by immunofluorescence staining in TCP, PEI600 and POCG groups. However, a few immature myotubes with MHC protein staining were tested in POCG-PEI600 groups (Fig. 4A). Therefore, we further tested the expression of proteins and mRNAs involved in POCG-PEI600 and TCP groups. To more broadly analyze changes in protein, we performed Western blot assay on MYOD and

MHC proteins following 7 days of incubation in DMEM with SB203580 or without SB203580 (Fig. 4B). And the bands of TCP and POCG-PEI600 groups were stronger than TCP + SB203580 and POCG-PEI600 + SB203580 groups, a sharp decline was seen when SB203580 was added. Especially, TCP + SB203580 groups did not obviously show the MYOD and MHC protein bands, however, POCG-
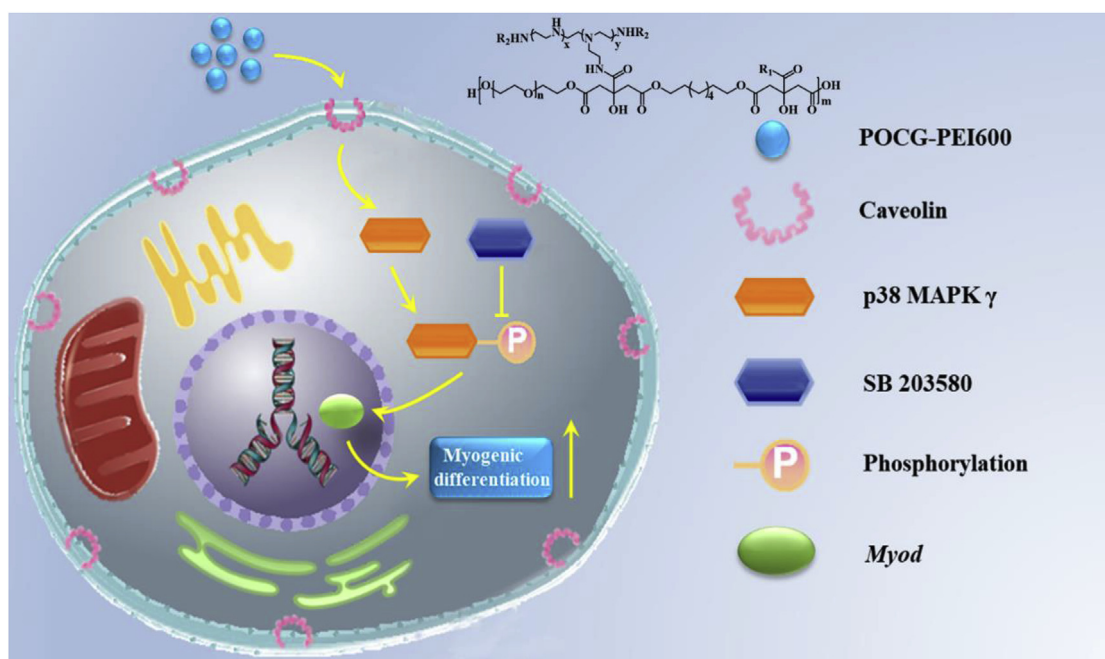
Scheme 1. Hypothetical molecular mechanism of the modulation of myogenic differentiation of C2C12 by POCG-PEI600 through p38 MAPK γ signaling pathway. SB 203580 was used as a p38 MAPK γ signaling pathway inhibitor.

PEI600 + SB203580 groups clearly revealed the protein bands (Fig. 4E and F). Subsequently, we detected the protein expression of signaling pathway during myoblast differentiation. There was slight fluctuation in levels of p38 when the inhibitor was mixed; however, we still found the clear protein band in TCP + SB203580 and POCG-PEI600 + SB203580 groups. In contrast, the band of phosphorylated -p38 (p-p38) was disappeared in TCP + SB 203580 groups (Fig. 4C and D). Comparing POCG-PEI600 + SB203580 groups and TCP + SB203580 groups, the band of POCG-PEI600 + SB203580 was clearer and stronger (Fig. 4B). We next evaluated *Myod* and *Mhc* expression that had been implicated in muscle cell fusion by examining the changes in their gene expression at different growth conditions. The real-time PCR showed that *Myod* and *Mhc* genes expression were declined under the influence of SB203580 in TCP, PEI600 and POCG groups. The genes expression of Myod and Mhc in POCG-PEI600 groups was higher than TCP, PEI600 and POCG groups (Fig. 4G). Thus, SB203580 prevents muscle fusion, however, POCG-PEI600 could still promote myogenic differentiation under the effect of SB203580. In a word, POCG-PEI600 can activate p38 MAPK γ signaling pathway through upregulating the level of p-p38 protein and facilitate myoblast differentiation efficiency (Scheme 1).

Several signaling pathways, such as Wnt, Notch, NF-kB, ERK1/2, FGF and TGF-β are responsible for regulating general skeletal muscle formation and reconstruction [47–49]. Then, some of these have been identified to play a crucial role in regulating myoblast differentiation. For instance, Wnt signaling pathway's role in skeletal muscle formation during development have been widely recognized and its versatile functions indicate its potential for therapeutic use [50,51].

Additionally, the p38 MAPK families are signal transducers that also promote muscle differentiation *in vitro* and influence muscle growth and repair *in vivo*, but only p38 MAPK γ directly affects myogenic transcription factors of the *Myod* family [52,53]. During differentiation, skeletal muscle C2C12 cells proliferate, migrate, and subsequently secede from the cell cycle associated with an increase in p38 MAPK γ signaling activity, align with each other, and fuse to form multi-nucleated myotubes [54,55]. The process can be followed by the increased expression of cytoskeletal components. Therefore, we speculated that the POCG-PEI600 *via* influencing p38 MAPK γ signaling pathway to regulate the C2C12 myoblast differentiation. We used a p38/MAP kinase inhibitor (SB 203580) that can prevent the p38 to phosphorylate. When C2C12 cells were cultured with SB203580 and POCG-PEI600 in inducting medium, the myoblast differentiation was still slightly underway. In contrast, only culturing with SB 203580 in inducting medium, the differentiation was almost suppressive. Subsequently, the results of immunofluorescence staining, mRNA and Western blot all illustrated that the POCG-PEI600 can enhance the phosphorylation of p38, which led to the improvement of the expression of *Myod* and the myoblast differentiation. Our study strongly suggests that the POCG-PEI600 can promote the skeletal muscle differentiation by activating the p38 MAPK γ signaling pathway.

3.4. Skeletal muscle tissue regeneration in vivo

Encouraged by the *in vitro* results, we performed a tibialis anterior muscle defect model for investigating the skeletal muscle regeneration capacity of POCG-PEI600 *in vivo*. After filling the defect by POCG-PEI600 hydrogel for 7 and 28 days, histological and molecular examinations were used to evaluate the skeletal muscle regeneration (Fig. 5 and Fig. 6). At 7 days, the newborn tissue had filled the defect in POCG-PEI600 group, however, the TCP and F127 hydrogel group still showed the obvious defects (Fig. 5A). The nuclei of mature myofibers are in the periphery of myofibers, and the nuclei in the cytoplasm center were regarded as the markers for the new born myofibers. As compared to TCP and F127 control, improved centronucleated myofibers were showed in the H.E. staining of the POCG-PEI600 group (Fig. 6B). The myofibers diameter, capillary density and centronucleated myofibers numbers was evaluated from the pictures of H.E. At days 7, there were no significant differences in diameter of myofibers (Fig. 5C). The capillary density and the number of centronucleated myofibers were significantly enhanced in the POCG-PEI600 group compared with TCP and F127 group (Fig. 5D and E). Then real time PCR was performed to evaluate the expression of *Myod* and *Mhc* genes in regenerative muscle tissue, in which the markers genes expression of POCG-PEI600 group was significantly enhanced (Fig. 5F).

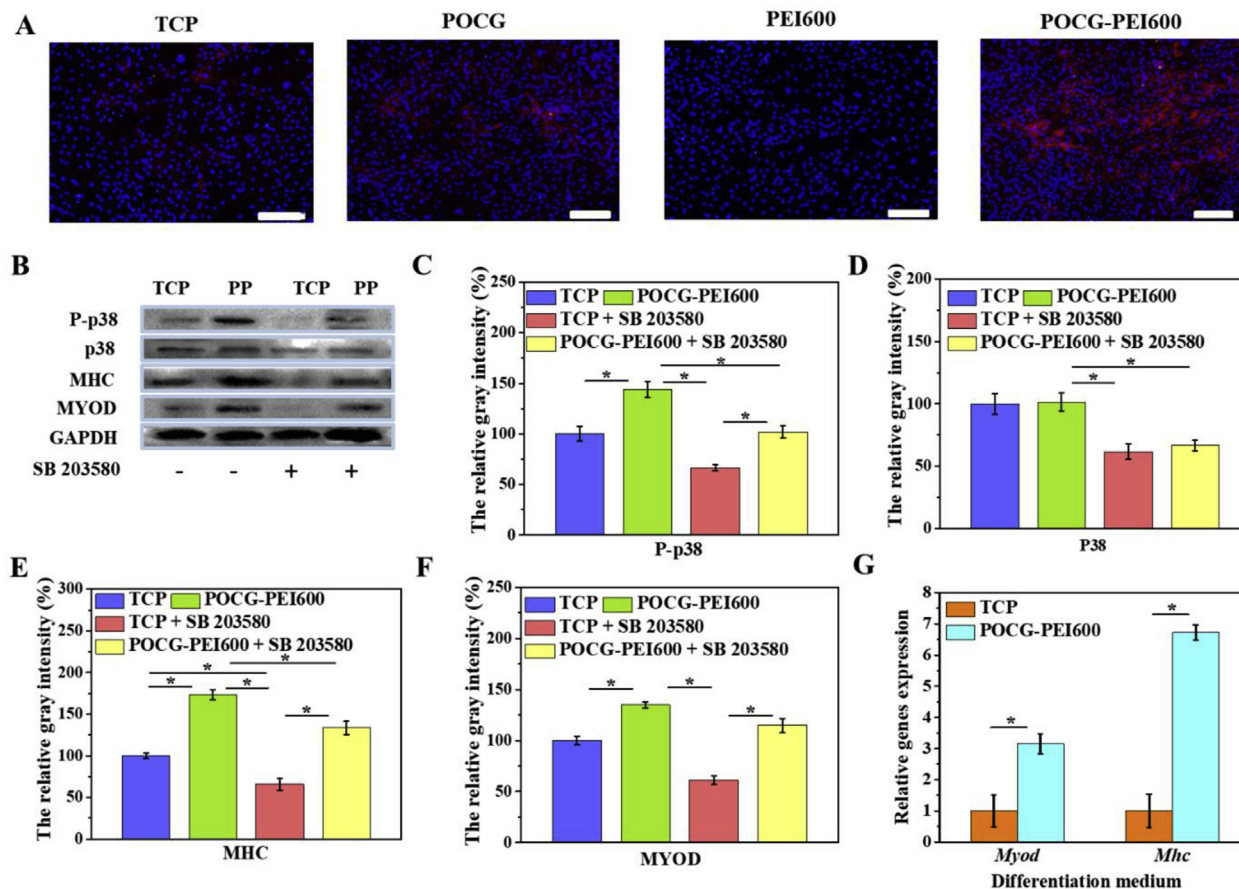After implantation for 28 days, there were still obvious defect in the

Fig. 4. Molecular mechanism analysis of myogenic differentiation of copolymers (40 μg/mL). (A) Immunofluorescence staining of MHC protein (red) in C2C12 cells on day 7 after incubation with copolymers in inhibitor-added myogenic differentiation medium (scale bar 200 μm, cell nuclei: blue); (B) Western blot analysis of MAPK pathway related proteins in C2C12 cells on day 7 after incubation with copolymers in inhibitor-added myogenic differentiation medium; (C–F) Quantitative gray level based on the Western blot bands for P-p38 (C), p38 (D), MHC (E) and MYOD (F) proteins expression; (G) *Myod* and *Mhc* gene expression in C2C12 cells on day 7 after incubation with POCG-PEI600 copolymers in inhibitor-added myogenic differentiation medium. All experiments were performed in triplicate (n = 4 per group, *$p < 0.05$, **$p < 0.01$). (For interpretation of the references to color in this figure legend, the reader is referred to the Web version of this article.)

TCP group and F127 group, however, the defect treated with the POCG-PEI600 hydrogel group showed a smooth surface similar with normal muscle tissue (Fig. 6A). The situation of regeneration was further confirmed by H.E. staining (Fig. 6B). The defect in POCG-PEI600 group had been completely repaired by new tissues compared with TCP and F127 group (Fig. 6B). Under the high magnification microscope, the tendency of diameter, capillaries and centronucleated myofibers numbers were consistent with previous results at days 7 (Fig. 6C, D and E). Comparing with TCP and F127 controls, the *Myod* and *Mhc* expression of POCG-PEI600 group were significantly improved (Fig. 6F). These results demonstrated that POCG-PEI600 could efficiently enhance the skeletal muscle regeneration *in vivo*.

3.5. Biodegradation and metabolism of POCG-PEI600 copolymer in vitro and in vivo

It is very necessary to evaluate the biodegradation performance of bioactive biomaterials for tissue regeneration. In this study, the biodegradation of POCG-PEI600 copolymer was carried out through analyzing the degradable product *in vitro* and the *in vivo* tissue distribution/metabolism. The biodegradable product of 1.8-octanediol was measured by the liquid chromatograph/mass spectrometer (Fig. S4). As the increase of degradation time, the amount of 1, 8-octanediol in the solution sustainably increased, demonstrating that the polymer was gradually degrading. The biodistribution and metabolism of POCG-PEI600

copolymer *in vivo* were determined using dye-labeled fluorescent imaging studies by the *in vivo* imaging system (Fig. S5). After 24 h of intravenous injection, as compared to other main organs, the significantly high fluorescent imaging on liver tissue was observed. Comparing with day 1, the fluorescent intensity on liver tissue was significantly decreased on day 3. Only slight fluorescence was seen in the lungs on day 7. At a later different point in time, there was no any fluorescence in main organs (Fig. S5A, Fig. S5B). These results demonstrated that POCG-PEI600 copolymer probably could be completely metabolized after about one week *in vivo*.

In this work, we investigated the myogenic differentiation and skeletal muscle regeneration performance and the detailed biodegradation *in vitro* and *in vivo* of POCG-PEI600 copolymer. It was found that POCG-PEI600 copolymer could significantly enhance the myogenic differentiation and myotube formation of myoblast through activating the potential signaling pathway of p38-MAPK, efficiently promote the full-thickness skeletal muscle tissue regeneration *in vivo*. The copolymer could be also be degraded into the small molecule monomers and metabolized completely in a short time. As compared to other biomedical polymers for skeletal muscle tissue engineering, the POCG-PEI600 copolymers possess special advantages. Firstly, the citric acid-based polymer has the similar elastomeric mechanical properties with the native skeletal muscle tissue, and most of other biodegradable artificial biopolymers do not have this property. Secondly, the skeletal muscle tissue has a fast growth period, which needs the fast biodegradation for
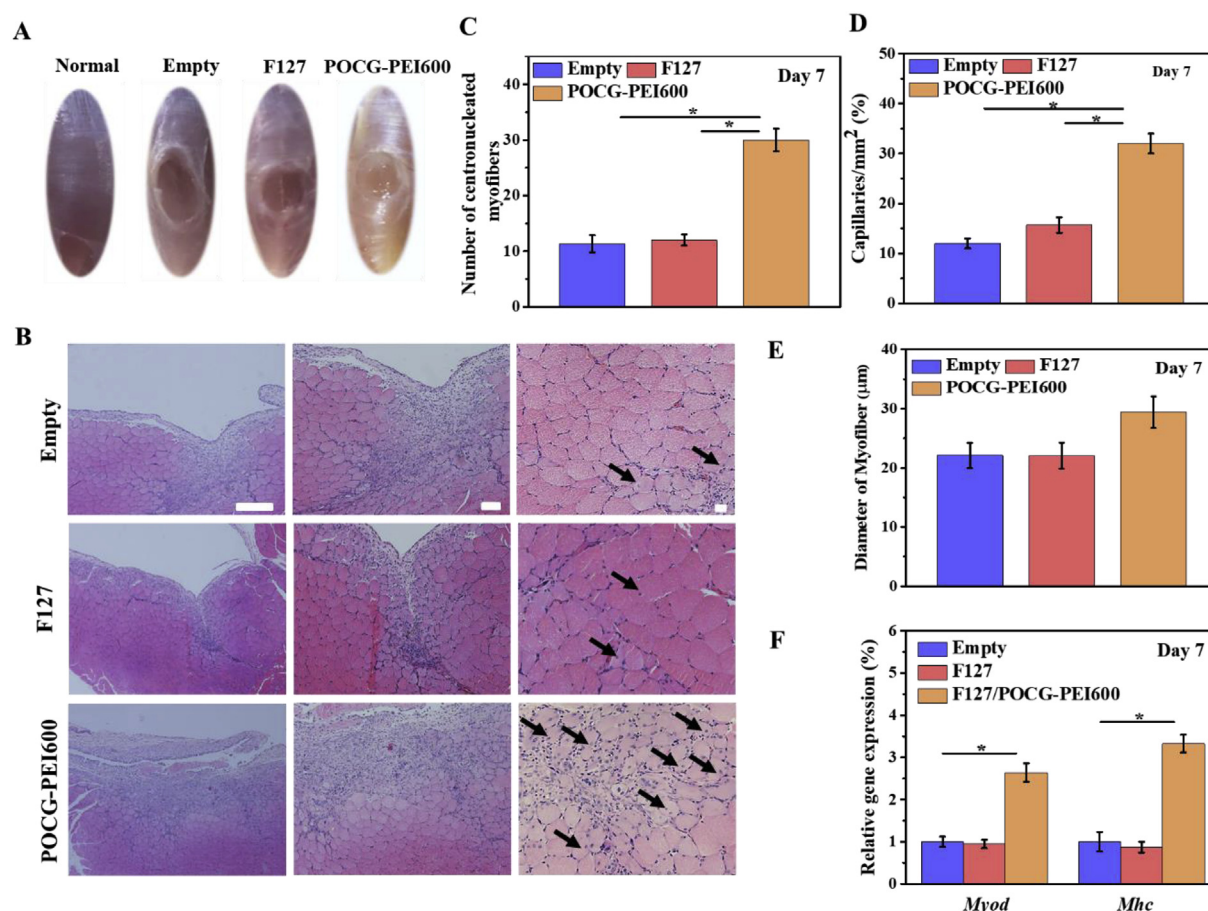
Fig. 5. *In vivo* **skeletal muscle tissue regeneration evaluation of POCG-PEI600 copolymer after implanted on the full-thickness muscle defect mice model for 7 days.** (A) Optical image of skeletal muscle defect on day 7, normal skeletal muscle was used as a control; (B) H.E. staining pictures of treated skeletal muscle tissue (scale bars = 50 μm, black arrow: centronucleated myofibers); (C) Analysis of formed myofibers diameter in the defect area; (D) Statistical data of capillary density in the regenerative site; (E) Numbers of centronucleated myofibers in repaired tissue; (F) *Myod* and *Mhc* gene expression in repaired muscle tissues. The empty and commercial F127 hydrogel treated groups were used as controls, $*p < 0.05$. $**p < 0.01$.

implanted biomaterials. Our POCG-PEI600 copolymers showed the fast biodegradation and metabolization *in vivo*, demonstrating the special advantage in skeletal muscle tissue engineering compared with other biodegradable polymers. Thirdly, POCG-PEI600 copolymers exhibited the enhanced myogenic differentiation and promoted muscle repair capacity, which has not been found on other biodegradable polymers. And previous work showed nanocarriers deliver growth factors to regulate the osteogenic differentiation of human bone marrow stem cells [56]. The nanocarriers with hydrogels as control programmed system release inductive factors to control the stem cells fate [57]. And our POCG-PEI600 offered an excellent alternative for the combine polymer materials with bioactive molecules to promote skeletal muscle tissue regeneration. Above all, the biodegradable POCG-PEI600 copolymers showed the promising potential in skeletal muscle tissue engineering.

4. Conclusion

In summary, this study found a biocompatible and bioactive biodegradable citric acid-based polymer (POCG-PEI600) which could accelerate the myoblast proliferation, myogenic differentiation and skeletal tissue regeneration *in vitro* and *in vivo*. POCG-PEI600 significantly enhanced the myoblasts differentiation through improving their myotubes formation, proteins levels and genes expressions, skeletal tissue formation *in vitro* and *in vivo*. Subsequent studies found that POCG-PEI600 could activate the p38 MAPK γ signaling pathway through upregulating the level of p-p38 protein which efficiently facilitates the

myoblast differentiation of C2C12 cell. POCG-PEI600 copolymer could be also biodegraded into small molecules and eliminated *in vivo*, suggesting their high biocompatibility and biosafety. This study suggests that POCG-PEI600 have great potential for safe and efficient muscle-related tissue regeneration.

CRediT authorship contribution statement

Yi Guo: Investigation, Writing - original draft. **Min Wang:** Investigation, Writing - original draft. **Juan Ge:** Data curation. **Wen Niu:** Data curation. **Mi Chen:** Formal analysis. **Wei Cheng:** Formal analysis. **Bo Lei:** Conceptualization, Supervision, Writing - review & editing.

Declaration of competing interest

The authors confirm that there are no any competing financial and conflict interests in this paper.
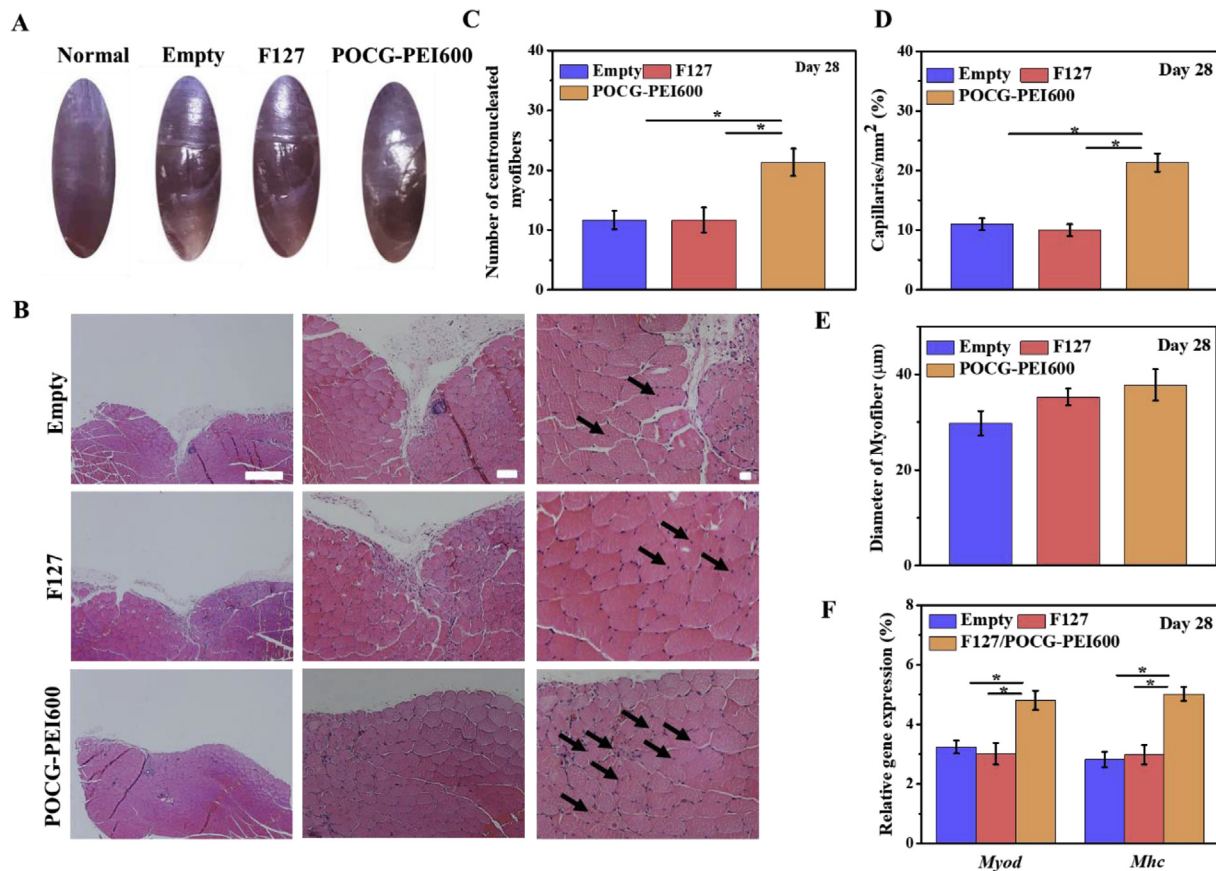
Fig. 6. *In vivo* skeletal muscle tissue regeneration evaluation of POCG-PEI600 copolymer after implanted on the full-thickness muscle defect mice model for 28 days. (A) Optical image of skeletal muscle defect on day 28, normal skeletal muscle was used as a control; (B) H.E. staining pictures of treated skeletal muscle tissue (scale bars = 50 μm, black arrow: centronucleated myofibers); (C) Analysis of formed myofibers diameter in the defect area; (D) Statistical data of capillary density in the regenerative site; (E) Numbers of centronucleated myofibers in repaired tissue; (F) *Myod* and *Mhc* gene expression in repaired muscle tissues. The Empty and commercial F127 hydrogel treated groups were used as controls, *$p < 0.05$. **$p < 0.01$.

Appendix A. Supplementary data

Supplementary data to this article can be found online at https://doi.org/10.1016/j.bioactmat.2020.04.004.

References

[1] S.S.K. Chan, R.W. Arpke, A. Filareto, N. Xie, M.P. Pappas, J.S. Penaloza, R.C.R. Perlingeiro, M. Kyba, Skeletal muscle stem cells from PSC-derived teratomas have functional regenerative capacity, Cell Stem Cell 23 (1) (2018) 74–86, https://doi.org/10.1016/j.stem.2018.06.010.

[2] S.S. Rayagiri, D. Ranaldi, A. Raven, N.I.F.M. Azhar, O. Lefebvre, P.S. Zammit, A.G. Borycki, Basal lamina remodeling at the skeletal muscle stem cell niche mediates stem cell self-renewal, Nat. Commun. 9 (1075) (2018) 56–68, https://doi.org/10.1038/s41467-018-03425-.

[3] M.B. Baghdadi, S. Tajbakhsh, Regulation and phylogeny of skeletal muscle regeneration, Dev. Biol. 433 (2) (2018) 200–209, https://doi.org/10.1016/j.ydbio.2017.07.026.

[4] M.N. Wosczyna, T.A. Rando, A muscle stem cell support group: coordinated cellular responses in muscle regeneration, Dev. Cell 46 (2) (2018) 135–143, https://doi.org/10.1016/j.devcel.2018.06.018.

[5] C.A. Cezar, D.J. Mooney, Biomaterial-based delivery for skeletal muscle repair, Adv. Drug Deliv. Rev. 84 (6) (2015) 188–197, https://doi.org/10.1016/j.addr.2014.09.008.

[6] G.C. Vigodarzere, S. Mantero, Skeletal muscle tissue engineering: strategies for volumetric constructs, Front. Physiol. 5 (58) (2014) 125–138, https://doi.org/10.3389/Fphys.2014.00362.

[7] C.M. Madl, S.C. Heilshorn, H.M. Blau, Bioengineering strategies to accelerate stem cell therapeutics, Nature 557 (7705) (2018) 335–342, https://doi.org/10.1038/s41586-018-0089-z.

[8] S. Ultimo, G. Zauli, A.M. Martelli, M. Vitale, J.A. McCubrey, S. Capitani, L.M. Neri, Influence of physical exercise on microRNAs in skeletal muscle regeneration, aging and diseases, Oncotarget 9 (24) (2018) 17220–17237, https://doi.org/10.18632/oncotarget.24991.

[9] Y.M. Xue, W. Niu, M. Wang, M. Chen, Y. Guo, B. Lei, Engineering a biodegradable multifunctional antibacterial bioactive nanosystem for enhancing tumor photothermo- chemotherapy and bone regeneration, ACS Nano 14 (1) (2020) 442–453, https://doi.org/10.1021/acsnano.9b06145.

[10] A. Marrella, T.Y. Lee, D.H. Lee, S. Karuthedom, D. Syla, A. Chawla, A. Khademhosseini, H.L. Jang, Engineering vascularized and innervated bone biomaterials for improved skeletal tissue regeneration, Mater. Today 21 (4) (2018) 362–376, https://doi.org/10.1016/j.mattod.2017.10.005.

[11] Y. Xi, J. Ge, M. Wang, M. Chen, W. Niu, W. Cheng, Y. Xue, C. Lin, B. Lei, Bioactive antiinflammatory antibacterial antioxidative silicon-based nanofibrous dressing enables cutaneous tumor photothermo-chemo therapy and infection-induced wound healing, ACS Nano (2020), https://doi.org/10.1021/acsnano.9b07173.

[12] K.L. Christman, Biomaterials for tissue repair, Science 363 (6425) (2019) 340–341, https://doi.org/10.1126/science.aar2955.

[13] F.J. Zhao, B. Lei, X. Li, Y.F. Mo, R.X. Wang, D.F. Chen, X.F. Chen, Promoting in vivo early angiogenesis with sub-micrometer strontium-contained bioactive microspheres through modulating macrophage phenotypes, Biomaterials 178 (5) (2018) 36–47, https://doi.org/10.1016/j.biomaterials.2018.06.004.

[14] S.M. Maffioletti, M.F.M. Gerli, M. Ragazzi, S. Dastidar, S. Benedetti, M. Loperfido, T. VandenDriessche, M.K. Chuah, F.S. Tedesco, Efficient derivation and inducible differentiation of expandable skeletal myogenic cells from human ES and patient-specific iPS cells (vol 10, pg 941, 2015), Nat. Protoc. 10 (9) (2015), https://doi.org/10.1038/nprot0915-1457d 1457-1457.

[15] J. Chal, O. Pourquie, Making muscle: skeletal myogenesis in vivo and in vitro, Development 144 (12) (2017) 2104–2122, https://doi.org/10.1242/dev.151035.

[16] S.H. Ku, C.B. Park, Myoblast differentiation on graphene oxide, Biomaterials 34 (8) (2013) 2017–2023, https://doi.org/10.1016/j.biomaterials.2012.11.052.

[17] C.Y. Zhao, H. Andersen, B. Ozyilmaz, S. Ramaprabhu, G. Pastorin, H.K. Ho, Spontaneous and specific myogenic differentiation of human mesenchymal stem cells on polyethylene glycol-linked multi-walled carbon nanotube films for skeletal

muscle engineering, Nanoscale 7 (43) (2015) 18239–18249, https://doi.org/10.1039/c5nr04303d.

[18] C.Y. Ning, Z.N. Zhou, G.X. Tan, Y. Zhu, C.B. Mao, Electroactive polymers for tissue regeneration: developments and perspectives, Prog. Polym. Sci. 81 (21) (2018) 144–162, https://doi.org/10.1016/j.progpolymsci.2018.01.001.

[19] Y.Z. Du, J. Ge, Y.N. Li, P.X. Ma, B. Lei, Biomimetic elastomeric, conductive and biodegradable polycitrate-based nanocomposites for guiding myogenic differentiation and skeletal muscle regeneration, Biomaterials 157 (5) (2018) 40–50, https://doi.org/10.1016/j.biomaterials.2017.12.005.

[20] X. Hu, S.H. Park, E.S. Gil, X.X. Xia, A.S. Weiss, D.L. Kaplan, The influence of elasticity and surface roughness on myogenic and osteogenic-differentiation of cells on silk-elastin biomaterials, Biomaterials 32 (34) (2011) 8979–8989, https://doi.org/10.1016/j.biomaterials.2011.08.037.

[21] J. Ge, K. Liu, W. Niu, M. Chen, M. Wang, Y.M. Xue, C.B. Gao, P.X. Ma, B. Lei, Gold and gold-silver alloy nanoparticles enhance the myogenic differentiation of myoblasts through p38 MAPK signaling pathway and promote in vivo skeletal muscle regeneration, Biomaterials 175 (5) (2018) 19–29, https://doi.org/10.1016/j.biomaterials.2018.05.027.

[22] J. Yang, A.R. Webb, G.A. Ameer, Novel citric acid-based biodegradable elastomers for tissue engineering, Adv. Mater. 16 (6) (2004) 511–517, https://doi.org/10.1002/adma.200306264.

[23] Y.Z. Du, M. Yu, J. Ge, P.X. Ma, X.F. Chen, B. Lei, Development of a multifunctional platform based on strong, intrinsically photoluminescent and antimicrobial silica-poly(citrates)-based hybrid biodegradable elastomers for bone regeneration, Adv. Funct. Mater. 25 (31) (2015) 5016–5029, https://doi.org/10.1002/adfm.201501712.

[24] J.S. Guo, G.B. Kim, D.Y. Shan, J.P. Kim, J.Q. Hu, W. Wang, F.G. Hamad, G. Qian, E.B. Rizk, J. Yang, Click chemistry improved wet adhesion strength of mussel-inspired citrate-based antimicrobial bioadhesives, Biomaterials 112 (2017) 275–286, https://doi.org/10.1016/j.biomaterials.2016.10.010.

[25] Y.X. Zhu, Z. Cankova, M. Iwanaszko, S. Lichtor, M. Mrksich, G.A. Ameer, Potent laminin-inspired antioxidant regenerative dressing accelerates wound healing in diabetes, Proc. Natl. Acad. Sci. U.S.A. 115 (26) (2018) 6816–6821, https://doi.org/10.1073/pnas.1804262115.

[26] S.Y. Zhang, A.M. Bellinger, D.L. Glettig, R. Barman, Y.A.L. Lee, J.H. Zhu, C. Cleveland, V.A. Montgomery, L. Gu, L.D. Nash, D.J. Maitland, R. Langer, G. Traverso, A pH-responsive supramolecular polymer gel as an enteric elastomer for use in gastric devices, Nat. Mater. 14 (10) (2015) 1065–1078, https://doi.org/10.1038/NMAT4355.

[27] U. Sharma, D. Concagh, L. Core, Y. Kuang, C.C. You, Q. Pham, G. Zugates, R. Busold, S. Webber, J. Merlo, R. Langer, G.M. Whitesides, M. Palasis, The development of bioresorbable composite polymeric implants with high mechanical strength, Nat. Mater. 17 (1) (2018) 96–118, https://doi.org/10.1038/NMAT5016.

[28] M.A. Hiob, G.W. Crouch, A.S. Weiss, Elastomers in vascular tissue engineering, Curr. Opin. Biotechnol. 40 (22) (2016) 149–154, https://doi.org/10.1016/j.copbio.2016.04.008.

[29] M.C. Serrano, E.J. Chung, G.A. Ameer, Advances and applications of biodegradable elastomers in regenerative medicine, Adv. Funct. Mater. 20 (2) (2010) 192–208, https://doi.org/10.1002/adfm.200901040.

[30] Y.W. Xi, Y. Guo, M. Wang, J. Ge, Y.L. Liu, W. Niu, M. Chen, Y.M. Xue, D.D. Winston, W.T. Dai, B. Lei, C. Lin, Biomimetic bioactive multifunctional poly(citrate-siloxane)-based nanofibrous scaffolds enable efficient multidrug-resistant bacterial treatment/non-invasive tracking in vitro/in vivo, Chem. Eng. J. 383 (11) (2020) 325–341, https://doi.org/10.1016/J.Cej.2019.123078.

[31] M. Wang, Y. Guo, M. Yu, P.X. Ma, C. Mao, B. Lei, Photoluminescent and biodegradable polycitrate-polyethylene glycol-polyethyleneimine polymers as highly biocompatible and efficient vectors for bioimaging-guided siRNA and miRNA delivery, Acta Biomater. 54 (6) (2017) 69–80, https://doi.org/10.1016/j.actbio.2017.02.034.

[32] M. Yu, Y.Z. Du, Y. Han, B. Lei, Biomimetic elastomeric bioactive siloxane-based hybrid nanofibrous scaffolds with miRNA activation: a joint physico-chemical-biological strategy for promoting bone regeneration, Adv. Funct. Mater. 30 (4) (2020) 268–281, https://doi.org/10.1002/Adfm.201906013.

[33] C.Y. Ma, X.G. Tian, J.P. Kim, D.H. Xie, X. Ao, D.Y. Shan, Q.L. Lin, M.R. Hudock, X.C. Bai, J. Yang, Citrate-based materials fuel human stem cells by metabonegenic regulation, Proc. Natl. Acad. Sci. U.S.A. 115 (50) (2018) E11741–E11750, https://doi.org/10.1073/pnas.1813000115.

[34] M. Chen, F.J. Zhao, Y.N. Li, M. Wang, X.F. Chen, B. Lei, 3D-printed photo-luminescent bioactive scaffolds with biomimetic elastomeric surface for enhanced bone tissue engineering, Mat. Sci. Eng. C-Mater. 106 (13) (2020) 145–157, https://doi.org/10.1016/J.Msec.2019.110153.

[35] K. Singh, F.J. Dilworth, Differential modulation of cell cycle progression distinguishes members of the myogenic regulatory factor family of transcription factors, FEBS J. 280 (17) (2013) 3991–4003, https://doi.org/10.1111/febs.12188.

[36] Y. Quan-Jun, H. Yan, H. Yong-Long, W. Li-Li, L. Jie, H. Jin-Lu, L. Jin, C. Peng-Guo, G. Run, G. Cheng, Selumetinib attenuates skeletal muscle wasting in murine cachexia model through ERK inhibition and AKT activation, Mol. Canc. Therapeut. 16 (2) (2017) 334–343, https://doi.org/10.1158/1535-7163.MCT-16-0324.

[37] A. Suzuki, R. Minamide, J. Iwata, WNT/beta-catenin signaling plays a crucial role in myoblast fusion through regulation of nephrin expression during development,

[38] S. Low, J.L. Barnes, P.S. Zammit, J.R. Beauchamp, Delta-like 4 activates Notch 3 to regulate self-renewal in skeletal muscle stem cells, Stem Cell. 36 (3) (2018) 458–466, https://doi.org/10.1002/stem.2757.

[39] A. Bohm, C. Hoffmann, M. Irmler, P. Schneeweiss, G. Schnauder, C. Sailer, V. Schmid, J. Hudemann, J. Machann, F. Schick, J. Beckers, M.H. de Angelis, H. Staiger, A. Fritsche, N. Stefan, A.M. Niess, H.U. Haring, C. Weigert, TGF-beta contributes to impaired exercise response by suppression of mitochondrial Key regulators in skeletal muscle, Diabetes 65 (10) (2016) 2849–2861, https://doi.org/10.2337/db15-1723.

[40] C.Q. Yi, D.D. Liu, C.C. Fong, J.C. Zhang, M.S. Yang, Gold nanoparticles promote osteogenic differentiation of mesenchymal stem cells through p38 MAPK pathway, ACS Nano 4 (11) (2010) 6439–6448, https://doi.org/10.1021/nn101373r.

[41] A.B. Lassar, The p38 MAPK family, a pushmi-pullyu of skeletal muscle differentiation, J. Cell Biol. 187 (7) (2009) 941–943, https://doi.org/10.1083/jcb.200911123.

[42] M. Wang, Y. Guo, Y.M. Xue, W. Niu, M. Chen, P.X. Ma, B. Lei, Engineering multifunctional bioactive citric acid-based nanovectors for intrinsical targeted tumor imaging and specific siRNA gene delivery in vitro/in vivo, Biomaterials 199 (6) (2019) 10–21, https://doi.org/10.1016/j.biomaterials.2019.01.045.

[43] J. Ge, K. Liu, W. Niu, M. Chen, M. Wang, Y.M. Xue, C.B. Gao, P.X. Ma, B. Lei, Gold and gold-silver alloy nanoparticles enhance the myogenic differentiation of myoblasts through p38 MAPK signaling pathway and promote in vivo skeletal muscle regeneration, Biomaterials 175 (3) (2018) 19–29, https://doi.org/10.1016/j.biomaterials.2018.05.027.

[44] S.C. Pohnert, M. Zhang, C. Gumbs, P. Rosenberg, R.S. Williams, Exercise stimulates PGC-1 alpha gene transcription in skeletal muscle through activation of the p38 MAPK pathway, Faseb. J. 18 (4) (2004) A364-A364 http://fasebj.org.

[45] M. Ihsan, J.F. Markworth, G. Watson, H.C. Choo, A. Govus, T. Pham, A. Hickey, D. Cameron-Smith, C.R. Abbiss, Regular postexercise cooling enhances mitochondrial biogenesis through AMPK and p38 MAPK in human skeletal muscle, Am. J. Physiol-Reg. I. 309 (3) (2015) R286–R294, https://doi.org/10.1152/ajpregu.00031.2015.

[46] A.A. Kazi, L. Hong-Brown, C.H. Lang, PRAS40 regulates protein synthesis, cell cycle, proliferation and myogenic differentiation in C2C12 myocytes, Faseb. J. 24 (2010), https://doi.org/10.1096/fasebj.24.1.

[47] J. Huang, C.L. Mo, L. Bonewald, M. Brotto, Wnt3a potentiates myogenesis in C2C12 myoblasts through changes of signaling pathways including Wnt and NF kappa B, J. Bone Miner. Res. 29 (1) (2014) S266–S267, https://doi.org/10.1002/jbmr.2126.

[48] R. Sartori, P. Gregorevic, M. Sandri, TGF beta and BMP signaling in skeletal muscle: potential significance for muscle-related disease, Trends Endocrinol. Metabol. 25 (9) (2014) 464–471, https://doi.org/10.1016/j.tem.2014.06.002.

[49] E.K. Enwere, J. Holbrook, R. Lejmi-Mrad, J. Vineham, K. Timusk, B. Sivaraj, M. Isaac, D. Uehling, R. Al-awar, E. LaCasse, R.G. Korneluk, TWEAK and cIAP1 regulate myoblast fusion through the noncanonical NF-kappa B signaling pathway, Sci. Signal. 5 (246) (2012), https://doi.org/10.1126/scisignal.2003086.

[50] M.S. Alexander, G. Kawahara, N. Motohashi, J.C. Casar, I. Eisenberg, J.A. Myers, M.J. Gasperini, E.A. Estrella, A.T. Kho, S. Mitsuhashi, F. Shapiro, P.B. Kang, L.M. Kunkel, MicroRNA-199a is induced in dystrophic muscle and affects WNT signaling, cell proliferation, and myogenic differentiation, Cell Death Differ. 20 (9) (2013) 1194–1208, https://doi.org/10.1038/cdd.2013.62.

[51] M. Karczewska-Kupczewska, M. Stefanowicz, N. Matulewicz, A. Nikolajuk, M. Straczkowski, Wnt signaling genes in adipose tissue and skeletal muscle of humans with different degrees of insulin sensitivity, J. Clin. Endocrinol. Metab. 101 (8) (2016) 3079–3087, https://doi.org/10.1210/jc.2016-1594.

[52] R.L. Qi, H. Liu, Q. Wang, J. Wang, F.Y. Yang, D.B. Long, J.X. Huang, Expressions and regulatory effects of P38/ERK/JNK mapks in the adipogenic trans-differentiation of C2C12 myoblasts, Cell. Physiol. Biochem. 44 (6) (2017) 2467–2475, https://doi.org/10.1159/000486169.

[53] J.D. Bernet, J.D. Doles, J.K. Hall, K.K. Tanaka, T.A. Carter, B.B. Olwin, p38 MAPK signaling underlies a cell-autonomous loss of stem cell self-renewal in skeletal muscle of aged mice, Nat. Med. 20 (3) (2014) 265–271, https://doi.org/10.1038/nm.3465.

[54] P. Brien, D. Pugazhendhi, S. Woodhouse, D. Oxley, J.M. Pell, p38 alpha MAPK regulates adult muscle stem cell fate by restricting progenitor proliferation during postnatal growth and repair, Stem Cell. 31 (8) (2013) 1597–1610, https://doi.org/10.1002/stem.1399.

[55] A. Cuenda, J.J. Sanz-Ezquerro, p38 gamma and p38 delta: from Spectators to Key Physiological Players, Trends Biochem. Sci. 42 (6) (2017) 431–442, https://doi.org/10.1016/j.tibs.2017.02.008.

[56] H.M. Kang, K.Y. Zhang, Q. Pan, S.E. Lin, D.S.H. Wong, J.M. Li, W.Y.W. Lee, B.G. Yang, F.X. Han, G. Li, B. Li, L.M. Bian, Remote control of intracellular calcium using upconversion nanotransducers regulates stem cell differentiation in vivo, Adv. Funct. Mater. 28 (41) (2018) 158–170, https://doi.org/10.1002/Afm.201802642.

[57] H.M. Kang, M. Kim, Q. Feng, S. Lin, K.C. Wei, R. Li, C.J. Choi, T.H. Kim, G. Li, J.M. Oh, L.M. Sian, Nanolayered hybrid mediates synergistic co-delivery of ligand and ligation activator for inducing stem cell differentiation and tissue healing, Biomaterials 149 (8) (2017) 12–28, https://doi.org/10.1016/j.biomaterials.2017.09.035.

Development 145 (23) (2018), https://doi.org/10.1242/dev.168351.